remote sensing

MDPI

Article

Monitoring Biophysical Variables (FVC, LAI, LC_{ab}, and CWC) and Cropland Dynamics at Field Scale Using Sentinel-2 Time Series

Reza Hassanpour [1], Abolfazl Majnooni-Heris [1,*], Ahmad Fakheri Fard [1] and Jochem Verrelst [2]

[1] Department of Water Engineering, Faculty of Agriculture, University of Tabriz, Tabriz 5166614766, Iran; r_hassanpour@tabrizu.ac.ir (R.H.); fakheri@tabrizu.ac.ir (A.F.F.)
[2] Image Processing Laboratory (IPL), University of Valencia, 46980 Valencia, Spain; jochem.verrelst@uv.es
* Correspondence: majnooni@tabrizu.ac.ir

Abstract: Biophysical variables play a crucial role in understanding phenological stages and crop dynamics, optimizing ultimate agricultural practices, and achieving sustainable crop yields. This study examined the effectiveness of the Sentinel-2 Biophysical Processor (S2BP) in accurately estimating crop dynamics descriptors, including fractional vegetation cover (FVC), leaf area index (LAI), leaf chlorophyll a and b (LC_{ab}), and canopy water content (CWC). The evaluation was conducted using estimation quality indicators (EQIs) and comprehensive ground throughout the entire growing season at the field scale. To identify soil and vegetation pixels, the spectral unmixing technique was employed. According to the EQIs, the best retrievals were obtained for FVC in around 99.9% of the 23,976 pixels that were analyzed during the growth season. For LAI, LC_{ab}, and CWC, over 60% of the examined pixels had inputs that were out-of-range. Furthermore, in over 35% of the pixels, the output values for LC_{ab} and CWC were out-of-range. The FVC, LAI, and LC_{ab} estimates agreed well with ground measurements (R^2 = 0.62–0.85), whereas a discrepancy was observed for CWC estimates when compared with ground measurements (R^2 = 0.51). Furthermore, the uncertainties of FVC, LAI, LC_{ab}, and CWC estimates were 0.09, 0.81 m^2/m^2, 60.85 $\mu g/cm^2$, and 0.02 g/cm^2 through comparisons to ground FVC, LAI, C_{ab}, and CWC measurements, respectively. Considering EQIs and uncertainty metrics, the order of the estimation accuracy of the four variables was FVC > LAI > LC_{ab} > CWC. Our analysis revealed that temporal variations of FVC, LAI, and LC_{ab} were primarily driven by field-scale events like sowing date, growing period, and harvesting time, highlighting their sensitivity to agricultural practices. The robustness of S2BP results could be enhanced by implementing a pixel identification algorithm, like embedding spectral unmixing. Overall, this study provides detailed, pixel-by-pixel insights into the performance of S2BP in estimating FVC, LAI, LC_{ab}, and CWC, which are crucial for monitoring crop dynamics in precision agriculture.

Keywords: canopy water content; fractional vegetation cover; leaf area index; leaf chlorophyll content; sentinel-2 biophysical processor; spectral unmixing

Citation: Hassanpour, R.; Majnooni-Heris, A.; Fakheri Fard, A.; Verrelst, J. Monitoring Biophysical Variables (FVC, LAI, LC_{ab}, and CWC) and Cropland Dynamics at Field Scale Using Sentinel-2 Time Series. *Remote Sens.* **2024**, *16*, 2284. https://doi.org/10.3390/rs16132284

Academic Editor: Dino Ienco

Received: 13 May 2024
Revised: 15 June 2024
Accepted: 18 June 2024
Published: 22 June 2024

1. Introduction

Continuous monitoring of crop growth throughout the growing season plays a critical role in increasing crop yields and minimizing costs and inputs for the agriculture industry [1]. Acquiring knowledge on biophysical variables, including fractional vegetation cover (FVC), leaf area index (LAI), canopy chlorophyll content (CCC), and canopy water content (CWC), is vital for comprehending agricultural ecosystems [2]. Accurately estimating these parameters is essential for land use and environmental applications, including precision agriculture, land surface monitoring, natural resource management, hydrological modeling, and global climate change monitoring [3–6]. The paramount importance of these parameters lies in their role in comprehending phenological stages and crop dynamics, which is crucial for optimizing agricultural practices and achieving sustainable crop yields.

FVC is defined as the ratio of vertically projected vegetation area to total surface area [7]. Through plant transpiration, photosynthesis, and surface albedo, FVC plays a pivotal role in climatic and biogeochemical cycles [8,9]. FVC is critical in monitoring vegetation growth status and understanding human-environment relationships (e.g., deforestation, land degradation, and desertification) [8,10]. LAI, representing one-half of the total green leaf area per unit of horizontal ground surface, is a crucial vegetation structural variable that is instrumental in the feedback of plants to the climate system [11]. Global Climate Observing System (GCOS) considers LAI to be an essential climatic variable [12] since it is a vital variable in key processes like energy and mass exchange, canopy interception, and gross photosynthesis [13]. Furthermore, key agricultural models utilize variables such as LAI as inputs, including the FAO-56 Penman–Monteith model, which calculates reference and potential crop evapotranspiration [14]. CCC is defined as the total amount of chlorophyll pigments in a contiguous group of plants per unit ground area, depicting the distribution of chlorophyll pigments across the three-dimensional canopy surface [15]. CCC is a product of leaf chlorophyll a and b (LC_{ab}) and LAI. CCC, as an essential indicator of plant health, is commonly used to evaluate plant disease, water deficits, and nutritional and environmental stresses [16,17]. CCC is one of the plant pigments that can help ecologists, farmers, and decision-makers assess the impact of climate change and other anthropogenic and natural factors on plant growth and ecosystem productivity [18]. CWC, which is defined as the amount of water in the vegetation per unit ground area, is another key biophysical attribute of terrestrial vegetation. CWC is a product of leaf water content and LAI. A profound understanding of the water status of vegetation and its variation pattern can effectively assist in the precise detection of the physiological status of vegetation [19–21]. Furthermore, CWC can furnish valuable insights for making judicious decisions regarding agricultural irrigation, facilitating drought monitoring assessment [22,23], as well as flood risk monitoring [24] and wildfire prevention [25,26].

Traditional measurements of crop biophysical variables are often laborious, time-consuming, and require continual updates while also being confined to small areas. As a promising alternative technique, satellite remote sensing has gained popularity for monitoring agricultural areas due to its ability to gather synoptic information on various temporal and spatial scales.

A wide range of approaches have been developed to retrieve crop biophysical variables from remote sensing data, primarily categorized into three main groups: (1) statistical methods, (2) physical-based methods, and (3) combined (hybrid) methods [27–29]. Statistical methods for retrieving crop biophysical variables can be either parametric or non-parametric [30]. Parametric regression methods rely on a pre-defined mathematical relationship between spectral observations and a specific biophysical variable, offering simplicity and low computational cost but limited generalizability [31,32]. Non-parametric methods adapt themselves to data without statistical assumptions, potentially improving accuracy but requiring field data, being sensor-specific, and at risk of overfitting with complex models [30,33,34].

Physical-based approaches utilize radiative transfer models (RTMs) to establish a cause-and-effect relationship between vegetation spectra and the target biophysical parameter [34,35]. These models account for variations in crop architecture, illumination, soil backgrounds, and viewing geometries, making them versatile for multiple operational applications [36] and flexible for diverse land cover conditions and sensor setups [37]. However, retrieving variables through RTM inversion can be challenging due to the ill-posed nature of the problem, where different combinations of input parameters can produce the same spectral signature [38]. Additionally, RTM inversion is computationally intensive, requires numerous leaf and canopy variables, and is affected by uncertainties from measurements and model assumptions [39]. There is also an inherent risk of oversimplifying canopy architecture in RTMs designed for operational applications [40].

Recent studies [41–43] have demonstrated that hybrid approaches, combining physically-based models with statistical methods, leverage the strengths of both approaches: physical

models provide a theoretical foundation and handle complex interactions between light and vegetation, while statistical methods offer flexibility, computational efficiency, and the ability to learn from data. The hybrid approach typically entails simulating canopy reflectance using RTMs and then using the simulated data to train parametric or non-parametric models to establish a link between spectral information and canopy parameters [44]. However, hybrid methods remain susceptible to sensor and atmospheric noise, measurement uncertainty, and the quality of the underlying RTMs. Despite these limitations, hybrid approaches have been successfully implemented in operational systems such as the Sentinel-2 Biophysical Processor (S2BP) through the Sentinel Application Platform (SNAP) and the Sentinel-2 for Agriculture (Sen2Agri) system [45,46]. These are neural networks providing biophysical parameter retrieval capabilities through model training for various satellite sensors, including PROBA-V, Sentinel-2 MSI, and Landsat-8 Operational Land Imager (OLI).

S2BP characteristics make It particularly suitable for cropland monitoring applications. First, it leverages Sentinel-2 data, which offers high spatiotemporal resolution and a rich set of spectral bands. This enables the generation of biophysical variables at a decametric spatial resolution and a 5-day interval, opening up new possibilities. Second, the processor is generic and does not require input data on specific land cover types. This makes it readily adaptable for retrieving vegetation biophysical variables at the global scale. Third, the S2BP algorithm has been integrated into the SNAP software (version 9.0.0, http://step.esa.int/main/download/snap-download/, accessed on 5 May 2024) and is publicly accessible for generating biophysical products [47,48]. This means that the S2BP tool can be easily utilized to derive biophysical estimates at scales ranging from field to global, as nneedsmay arise.

Despite the promising performance of Sentinel-2 biophysical estimates, previous studies have encountered several limitations that require attention in order to fully assess their capabilities. First, most validation studies have concentrated on specific biophysical variables like LAI or chlorophyll content [6,49]. Second, validation efforts have typically been conducted over a restricted period, regardless of the duration of the plan's entire growing season and phenological stages. These knowledge gaps underscore the need for a comprehensive evaluation of Sentinel-2 vegetation biophysical estimates based on ground measurements and estimation quality indicators (EQIs) to gain a broader understanding of their performance. Altogether, this study aims to: (i) evaluate the estimation accuracy of FVC, LAI, LC_{ab}, and CWC derived from S2BP throughout the entire corn growing season, utilizing comprehensive ground measurements and EQIs at the field scale with detailed pixel-by-pixel analysis; (ii) compare the reliability of four biophysical estimates, i.e., FVC, LAI, LC_{ab}, and CWC; and (iii) identify cropland dynamics (including sowing, growing, and harvest dates) using temporal variations of FVC, LAI, LC_{ab}, and CWC.

2. Materials and Methods

2.1. Study Area

The study area was a field with corn (*Zea mays* L., cultivar single cross 704) of approximately 10 ha, located in the Agricultural Research Station of Tabriz University in East Azerbaijan Province, Iran (Figure 1). The climate is cold and semi-arid, with an average annual precipitation of 285 mm and an average annual temperature of 12.1 °C. The field data used in this study were gathered during the growing season (June to October) of 2018. The field's soil texture was sandy clay loam (54.8% sand, 21.4% silt, and 23.8% clay), and it was irrigated using a center pivot irrigation system.

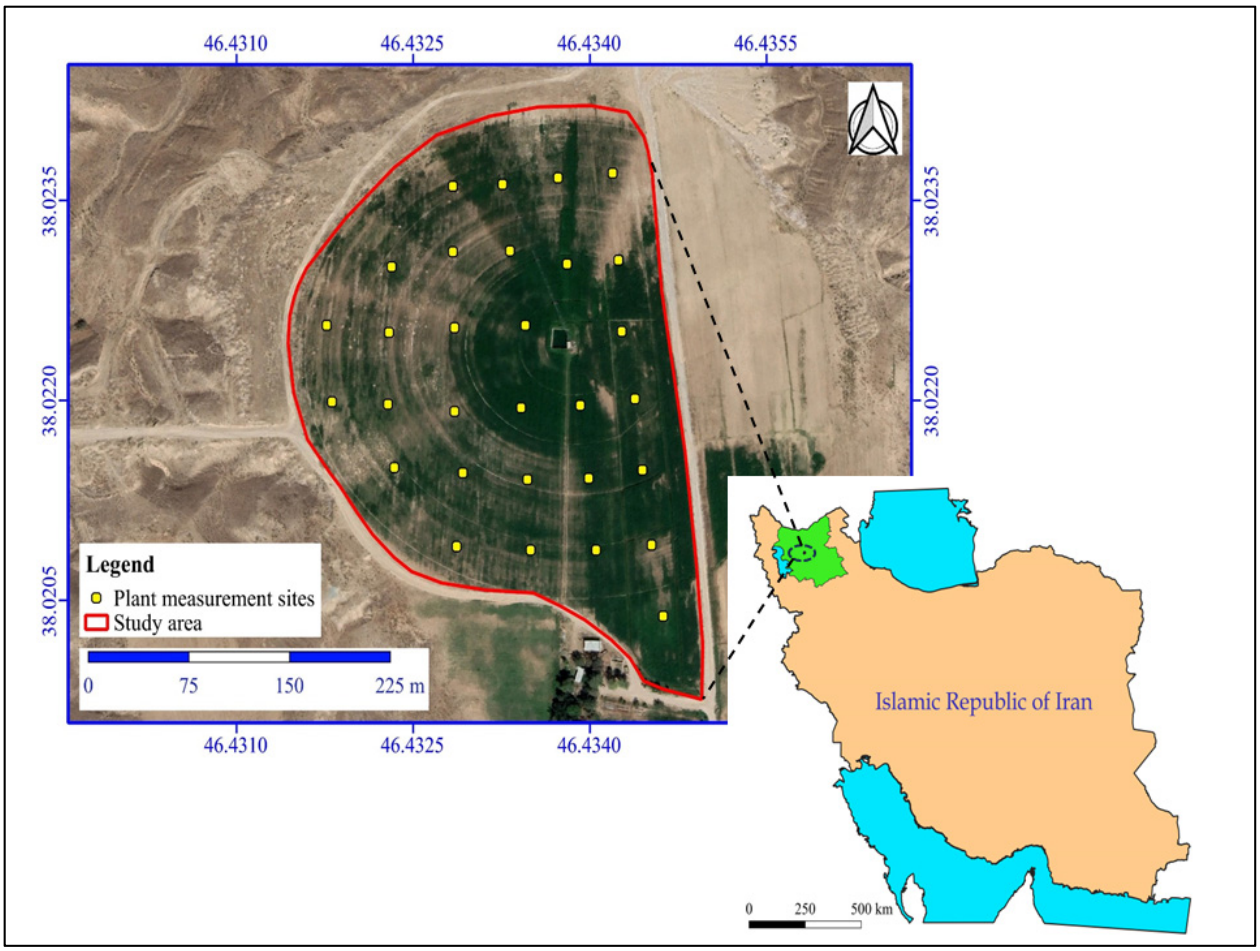

Figure 1. Geographical location of study area.

2.2. Ground Truth Data

The in situ measurements were collected following the Validation of Land European Remote Sensing Instruments (VALERI) field protocol [50], which is a widely recognized sampling strategy for high spatial-resolution satellite imagery. This protocol advocates the use of elementary sampling units (ESUs) of 20 m × 20 m for each measuring plot. Within the field, ESUs were selected while ensuring a minimum distance of 20 m between adjacent ESUs and the edges of the field. To account for the spatial FVC, LAI, LC_{ab}, and CWC variability within each ESU, the measuring points were arranged in a square spatial sampling pattern with five random measurements at each of the five points (A, B, C, D, and E) within each ESU (Figure 2). This sampling scheme allowed for the derivation of statistically averaged FVC, LAI, LC_{ab}, and CWC estimates for each ESU. The center of each ESU (sampling point A) was precisely located using a global positioning system (GPS), ensuring accurate matching of the mean FVC, LAI, LC_{ab}, and CWC measurements with the corresponding estimates derived from Sentinel-2 data. This precise geolocation facilitated the validation and comparison of field-based measurements with satellite-derived data.

FVC and LAI were determined using digital hemispherical photographs and Can-Eye imaging software (version 6.45) following the SMAPVEX16-MB protocol, which is aligned with the Canada Centre for Remote Sensing (CCRS) protocol for crops [51]. For each ESU, based on the photography design for a homogeneous canopy [52], 12 downward-looking photos were captured from above the canopy using a Digital Hemispheric Photos camera (Canon EOS 5D Mark II) with a fish eye lens at A, B, C, and D points of the ESU and the distance between them. All 12 photos were processed together to provide one estimate of FVC and LAI per ESU.

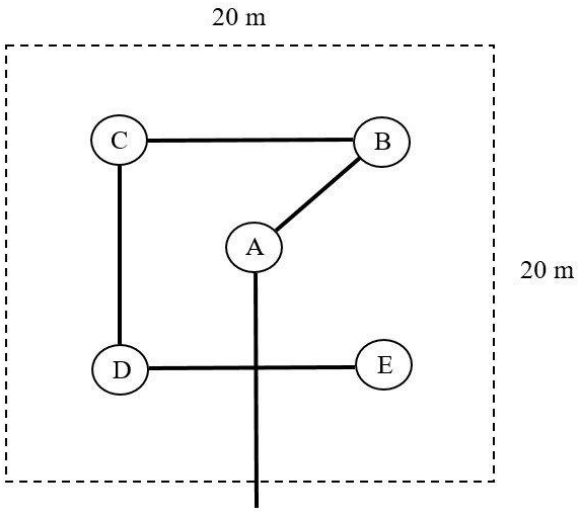

Figure 2. Validation of the Land European Remote Sensing Instruments (VALERI) sampling approach for each elementary sampling unit (ESU). A, B, C, D and E represent the measurement or sampling points within each ESU.

The leaf chlorophyll content, on the other hand, was taken by the CL-01 Chlorophyll Content Meter (Hansatech Instruments Ltd., Norfolk, UK). CL-01 measures relative chlorophyll content—the chlorophyll content index (CCI) [53]. To evaluate the performance of the S2BP in predicting LC_{ab} ($\mu g/cm^2$), the measured CCI values (−) were converted to $\mu g/cm^2$ using a laboratory-developed CCI-LC_{ab} function.

CWC (g/cm^2) was determined using gravimetric methods [51,54] from Equations (1) and (2):

$$CWC = EWT \times LAI \quad (1)$$

$$EWT = \frac{FW - DW}{A} \quad (2)$$

where *EWT* is equivalent to water thickness (g/cm^2) and *LAI* is the leaf area index at each ESU. To measure *EWT*, leaf samples were collected from the 10 young, fully developed leaves at the top of the canopy at each ESU point (A, B, C, D, E), resulting in a total of 50 leaf samples per ESU. The leaf samples were placed in sealed plastic bags and transferred to a cool dark container (with ice water) to prevent water loss during transport to the laboratory. In the laboratory, leaf discs were prepared using a sharp-edged steel tube with a 2.2 cm internal diameter, and their fresh weight (*FW*) was measured with a sensitive balance. The samples were then transferred to an oven at 75 °C for 24 h and re-weighed (*DW*). Consequently, the measured *EWT* at each ESU was calculated as the average of the 50 values obtained.

2.3. Satellite Data Acquisition and Processing

Sentinel-2 satellite data were utilized in this study. Sentinel-2 is a mission of the European Space Agency (ESA) for global monitoring with high spatial and temporal resolution. This mission comprises a constellation of two polar-orbiting satellites (2A and 2B) positioned in the same sun-synchronous orbit, phased at 180° to each other. Each satellite acquires imagery every ten days, and their combined efforts achieve a revisit frequency of every five days, ensuring comprehensive coverage of Earth's land surfaces and coastal zones. Each satellite is equipped with a Multi-Spectral Imager (MSI) that collects data in 13 spectral bands, including four bands at 10 m, six bands at 20 m, and three bands at 60 m spatial resolution, ranging from the visible to the shortwave infrared region (400–2500 nm) (Table 1) [55].

Table 1. Sentinel-2 spectral bands and their characteristics [55].

Band	B1	B2	B3	B4	B5	B6	B7	B8	B8a	B9	B10	B11	B12
Band center (nm)	443	490	560	665	705	740	783	842	865	945	1375	1610	2190
Bandwidth (nm)	20	65	35	30	15	15	20	115	20	20	30	90	180
Spatial resolution (m)	60	10	19	10	20	20	20	10	20	60	60	20	20

Sentinel-2 images can be downloaded for free on the Copernicus Data Space Ecosystem website (https://dataspace.copernicus.eu/, accessed on 5 May 2024). In this study, all cloud-free images available during the corn-growing season were downloaded (Table 2). Sentinel-2 satellite images are processed through several stages to enhance their accuracy and usability. These processing levels are known as Level-0, Level-1A, Level-1B, Level-1C, and Level-2A. The Level-1C products, which have already undergone radiometric and geometric corrections, were downloaded. Since these products only provide top-of-atmosphere (TOA) reflectance, atmospheric correction is necessary. The Sen2Cor processor (version 2.8.0, https://step.esa.int/main/snap-supported-plugins/sen2cor/sen2cor_v2-8/, accessed on 5 May 2024) was employed within the Sentinel Application Platform (SNAP) software (version 9.0) to convert the TOA reflectance data into atmospherically corrected surface reflectance (Level-2A). The reflectance of the used bands (bands 3–7, 8a, and 11–12) was resampled to the 20-m grid using the nearest neighbor approach integrated into SNAP in order to match the ground ESU due to the various spatial resolutions (10- and 20-m) for these bands.

Table 2. Sentinel-2 images used in this study.

No. of Images	Acquisition Dates (2018)
32	20 April, 25 April, 4 May, 9 May, 19 May, 24 May, 9 March, 19 March, 8 June, 13 June, 18 June, 23 June, 28 June, 3 July, 13 July, 18 July, 28 July, 2 August, 7 August, 17 August, 22 August, 27 August, 1 September, 6 September, 11 September, 16 September, 21 September, 26 September, 1 October, 11 October, 16 October, 21 October

2.4. Estimating Biophysical Variables

The Sentinel-2 Biophysical Processor (S2BP) tool, integrated into SNAP, was utilized to retrieve biophysical variables, including FVC, LAI, LC_{ab}, and CWC. The theoretical algorithms of S2BP are developed using a neural network approach [45]. The neural network models were developed following three key steps: (1) utilizing the PROSAIL model to generate training datasets, (2) calibrating the neural network, and (3) using the trained neural network to estimate biophysical variables (Figure 3). PROSAIL is a combination of the SAIL (canopy bidirectional reflectance model) and PROSPECT (leaf reflectance and transmittance model). It connects the directional dimension of reflectance, which is mostly connected to the architecture of the canopy, to the spectral dimension of reflectance, which, in turn, is primarily related to the biochemical composition of the leaves [44]. The values of the input variables for the PROSPECT model are based on prior knowledge from the literature and the specific type of vegetation. The soil reflectance for the SAIL model is primarily derived from a soil reflectance database that includes a wide range of soil properties. The LAI, average leaf angle distributions, and hot spot parameters are obtained from the VALERI dataset. PROSAIL incorporates directional information, such as solar zenith angle, view zenith angle, and the relative azimuth angle between solar and view, to simulate canopy reflectance. More details can be found in [45].

The dataset derived from PROSAIL is subsequently used to train the neural network. Eight spectral bands (3–7, 8a, 11, 12) from the Sentinel-2 MSI are used to retrieve biophysical variables. The neural network consists of 3 layers: the input layer, the hidden layer, and the output layer. The input layer consists of 11 neurons representing 11 input variables: canopy reflectance of 8 bands and the cosine of 3 angles related to the geometry of the observation (solar zenith angle, view zenith angle, and relative azimuth angle between

solar and view). The hidden layer contains five neurons with tangent sigmoid transfer functions. Each FVC, LAI, LC_{ab}, and CWC is derived from the output layer of a separate neural network equipped with a dedicated linear transfer function, implying that a total of four neural networks are required to generate these retrievals.

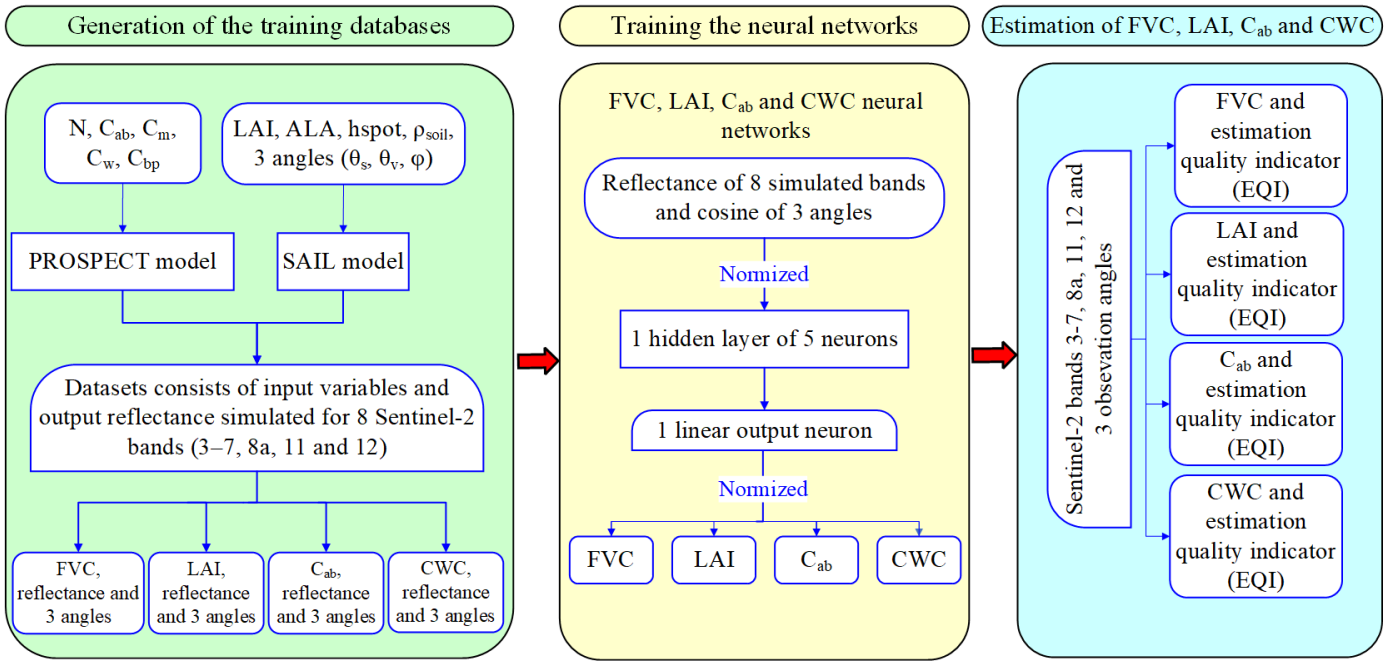

Figure 3. The framework of the biophysical variables retrieval algorithm using Sentinel-2 imagery. In the PROSPECT model, N, C_{ab}, C_w, C_m, and C_{bp} represent the mesophyll structure index, chlorophyll content (μg/cm^2), dry matter content (g/cm^2), water content (g/cm^2), and brown pigment content for leaf, respectively. In the SAIL model, LAI, ALA, h_{spot}, ρ_{soil}, θ_s, θ_v, and s_v correspond to leaf area index (m^2/m^2), average leaf angle (○), hot spot parameter, soil reflectance, solar zenith angle (○), view zenith angle (○), and the relative azimuth angle between solar and view (○), respectively [45].

Estimation Quality Assessment

The outputs of S2BP include the neural network-derived FVC, LAI, LC_{ab}, and CWC. Each parameter estimate is also accompanied by its corresponding estimation quality indicator (EQI) (Figure 3), the so-called "quality flags", which facilitates a more nuanced comprehension of the spatial distribution of uncertainties. When the inputs fall outside the convex hull defined by the simulated reflectance values of the training database, known as the definition domain, a specific 'input out-of-range' flag is raised. The convex hull is represented by a hypercube with the same dimensions as the neural network inputs. Each dimension, corresponding to a specific neural network input, ranges between minimum and maximum values. If the artificial neural network estimates biophysical variables beyond their defined range, the product value will be adjusted to the nearest boundary of the range, either the minimum or maximum accepted values. Due to uncertainties from various sources related to the inputs and algorithm calibration, a tolerance is established before raising the 'output out-of-range' flag.

Therefore, these qualitative indicators allow the user to properly 'weigh' the data within its application according to the confidence they put therein. The estimates are categorized into three groups based on their EQI values (Figure 4), as follows:

- Best retrievals: EQI = 0, indicating that both input and output variables fall within their valid ranges.
- Input out-of-range: EQI = 1, implying that one or more input variables exceed their valid ranges. This indicates that either the input reflectance have problems (cloud

contamination, poor atmospheric correction, shadow) or that the application of the algorithm could result in unreliable results.

- Output out-of-range: EQI > 1, suggesting that the estimated variables exceed its nominal range of variation.

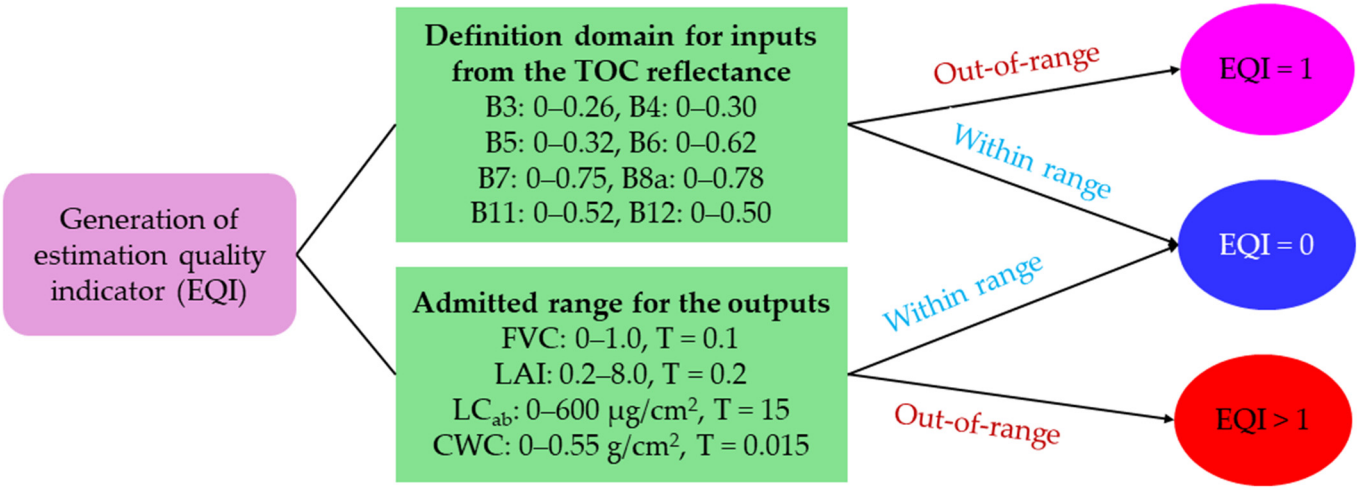

Figure 4. Flowchart illustrating the algorithm of estimation quality indicators (EQIs) for fractional vegetation cover (FVC), leaf area index (LAI), leaf chlorophyll a and b (LC_{ab}), and canopy water content (CWC). The TOC, B, and T denote top of canopy reflectance, Sentinel-2 bands, and output range tolerance, respectively.

2.5. Pixel Identification Using Spectral Unmixing

Mixed pixels exist widely in the remotely sensed images of an agricultural field throughout the growing season, particularly during the early and late stages. In order to obtain more reliable information about the biophysical variables of the cropland under these circumstances and to properly evaluate the quality of the estimates, spectral unmixing is required to determine the composition of the mixed pixels in terms of soil and vegetation proportions. For this purpose, the linear spectral unmixing tools in SNAP were used. The unmixing algorithms are based on the following linear mixing model, which assumes that a spectrum is a linear superposition of endmembers:

$$R_b = \sum_{i=1}^{n} f_{i,b} \times r_{i,b} + e_b \quad (3)$$

where R_b is the reflectance of the mixed pixel at band b, f_i is the proportion of endmember i, $r_{i,b}$ is the reflectance of endmember i in band b, n is the number of endmembers, and e_b is the fitting error at band b [56]. The inputs of the linear spectral unmixing algorithm are the pure spectra of the individual endmembers in the mixed pixel. Since the end members in the study area were soil and vegetation, we derived their pure spectrum from the pixels with bare soil and full vegetation, respectively, and proceeded with the process. The outputs represented the proportion of soil and vegetation as well as the unmixing error.

Since no specific threshold exists in the literature to identify soil or vegetation pixels based on their proportions, we employed normalized difference vegetation index (NDVI) thresholds. The Sentinel-2 surface reflectance products Algorithm Theoretical Basis Document (ATBD) guided the identification of vegetation or soil pixels using NDVI values [57]. This document introduced an NDVI threshold of 0.4 to classify soil and vegetation pixels.

In our dataset, we established a relationship between vegetation proportion (VP) and NDVI ($VP = 0.906NDVI - 0.063$, $R^2 = 0.94$, $N = 8991$) and set a 30% VP threshold to differentiate between soil and vegetation pixels, a method further supported by field visual observations. To distinguish between sparse and dense vegetation (60% VP), we used an NDVI threshold of 0.75 alongside field visual assessments.

2.6. Mapping Biophysical Variables

To assess the ability of S2BP to monitor spatial and temporal variations in biophysical variables and crop dynamics, FVC, LAI, LC_{ab}, and CWC maps were prepared alongside EQIs maps across six distinct growth stages (sowing, establishment, end of vegetative growth, flowering, senescence, and harvesting). This was accomplished using QGIS 3.32.

2.7. Accuracy Assessment

The S2BP-derived biophysical variables were compared with ground measurements through a regression model. The accuracy of the estimates was assessed using four well-established goodness-of-fit measures: root mean square error (RMSE) [58], bias [59], Nash–Sutcliffe model efficiency coefficient (NSE) [60], and coefficient of determination (R^2) [61]. Mathematically, the estimates are more accurate when the RMSE and bias values are closer to 0 and the values of NSE and R^2 are closer to 1.

3. Results

3.1. Pixel Identification

The cropland soil and vegetation pixels were identified using spectral unmixing tools and by analyzing the pixel endmember proportion throughout the growing season. To achieve this, the proportions of soil and vegetation in the pixels were determined using the aforementioned tool. Pixels with a vegetation proportion (VP) of less than 30% are referred to as soil pixels, pixels with a VP between 30 and 60% are sparse vegetation pixels, and pixels with a VP of more than 60% are referred to as dense vegetation pixels. With this classification, of the total 23,976 pixels examined during the growing season, about 51% of the pixels were classified as soil pixels, and about 49% of the pixels were classified as sparse and dense vegetation pixels (Table 3).

Table 3. The evaluation results of the soil and vegetation pixel identifications based on the spectral unmixing and pixel vegetation proportion at (total pixels = 23,976).

Pixel Type	Soil	Sparse Vegetation	Dense Vegetation
Vegetation proportion (%)	0–30	30–60	60–100
Frequency	12,422 (51.81%)	6393 (26.67%)	5161 (21.52%)
Unmixing error		0.034	

Figure 5 indicates the frequency of soil and vegetation pixels during the growing season. It is obvious that at the beginning of the growing season and before the plant is established in the field (3 July), the abundance of soil pixels is high, but after that date and with the development of the plant, the abundance of vegetation pixels increases. In the middle of the growing season (2 August to 1 October), most pixels in the field are vegetation pixels. At the end of the growing season (11 October), the number of soil pixels in the field predominates anew.

3.2. Assessment of Biophysical Variables Estimates Using Estimation Quality Indicators

Figure 6 indicates the overall estimation quality for FVC, LAI, LC_{ab}, and CWC. For the 23,976 pixels in our study, the S2BP achieved the best retrieval (EQI = 0) for FVC at 23,943 pixels (99.86%) and for LAI, LC_{ab}, and CWC at 4828 pixels (about 20%). At only 33 pixels (0.14%), the FVC value was out-of-range (EQI = 2). Based on the spectral unmixing results (Section 3.1) and field observations, in these 33 pixels, the proportion of vegetation was zero, in other words, they were soil pixels. When estimating the LAI, we had no out-of-range output, but for about 80% of the pixels, the inputs were out-of-range (EQI = 1, meaning that the input values deviated from the training data). For LC_{ab}, the output was out-of-range for about 17% of the pixels (EQI = 3) and the input was out-of-range (EQI = 1) for about 63% of the pixels. However, for 3991 pixels with EQI 3, the LC_{ab} value was zero.

In these 3991 pixels, the pixel proportion of vegetation was very low (<28%) and the LC_{ab} value was zero, which met expectations. According to our classification, these are soil pixels. Regarding CWC, 861 pixels with an EQI of 9 exhibited negative, occurring in pixels with a vegetation proportion below 23%. Additionally, 3274 pixels had an EQI of 3, found in pixels with a vegetation proportion below 32%.

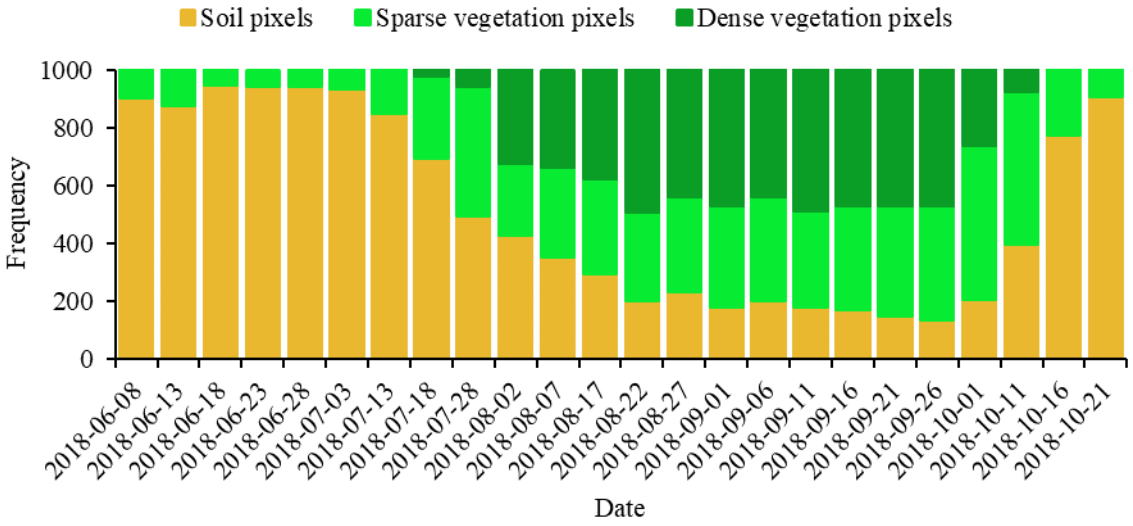

Figure 5. Frequency of soil and vegetation pixels during the growing season.

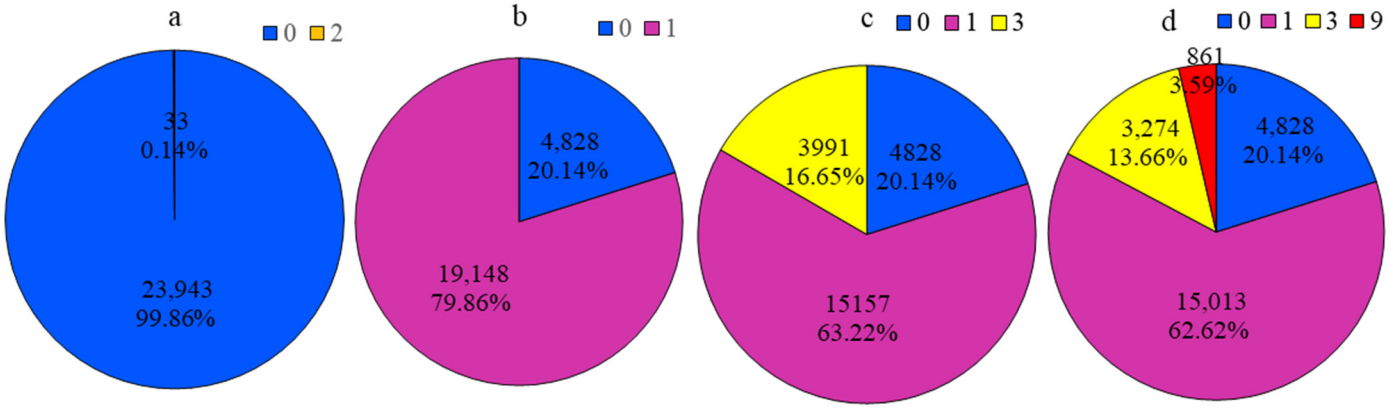

Figure 6. Overall estimation quality for fractional vegetation cover (**a**), leaf area index (**b**), leaf chlorophyll a and b (**c**), and canopy water content (**d**) at all 23,976 pixels during the growing season. 0: best retrieval, 1: input out-of-range, >1: output out-of-range.

Figure 7 indicates the temporal variations of EQIs for FVC, LAI, LC_{ab}, and CWC. The best retrievals for FVC were achieved at all pixels for all dates except 28 June and 3 July. However, for LAI, LC_{ab}, and CWC, a high frequency of input and out-of-range estimates was observed on dates with a high number of soil pixels (as shown in Figure 7). As vegetation cover in the field increases, the number of out-of-range estimates decreases, leading to improved retrievals.

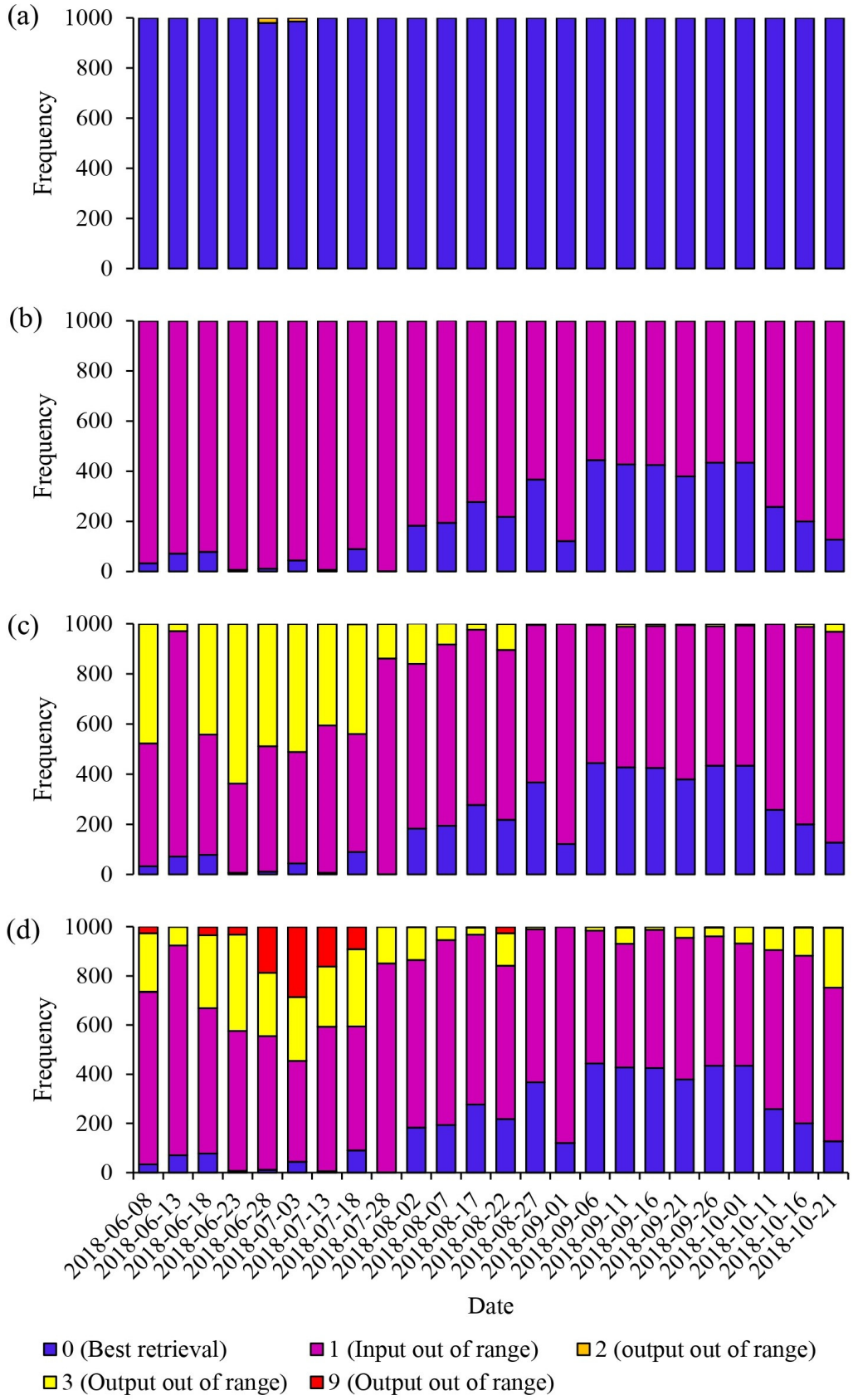

Figure 7. Frequency of estimation quality indicators (EQIs) for fractional vegetation cover (**a**), leaf area index (**b**), chlorophyll (**a**,**b**) concentration (**c**), and canopy water content (**d**) during the growing season.

3.3. Validation of Biophysical Variables by In-Situ Measurements

To assess the accuracy of the S2BP-derived biophysical variables, we conducted field measurements of FVC, LAI, LC_{ab}, and CWC at four distinct growth stages. Table 4 summarizes the statistical characteristics of these parameters. This wide range of biophysical parameter values enabled a comprehensive evaluation of the accuracy of S2BP estimates under various growth conditions.

Table 4. Statistical description of measured biophysical variables on 18 July, 22 August, 1 September, and 1 October 2018.

Parameters	Unit	Minimum	Maximum	Mean	St. Dev
Fractional vegetation cover (FVC)	-	0.07	0.97	0.52	0.23
Leaf area index (LAI)	m^2/m^2	0.23	5.82	2.17	1.27
Leaf chlorophyll a and b (LC_{ab})	$\mu g/cm^2$	0	380.56	104.33	74.82
Canopy water content (CWC)	(g/cm^2)	0.0054	0.109	0.040	0.028

Figure 8 illustrates the punctual comparisons and density scatter plots for FVC, LAI, LC_{ab}, and CWC between S2BP estimates and corresponding in-situ measurements. In terms of FVC accuracy, Figure 8a reveals that S2BP performed well. This conclusion is supported by the observation that the linear regressions versus in-situ measurements closely follow the 1:1-line (slope = 0.92). No significant bias (bias = −0.03) was observed for FVC comparison between S2BP estimates and in-situ measurements. Overall, among the biophysical variables, FVC estimates prevailed with the highest level of consistency against in-situ measurements, with an RMSE of 0.09, NSE of 0.81, and R^2 of 0.85.

In terms of LAI comparison (Figure 8b), the estimates showed quite good agreement with in-situ measurements, as indicated by the low scattering of data and a good R^2 of 0.69. Additionally, the bias was small (0.31 m^2/m^2), and the uncertainty was low with an RMSE of 0.81 m^2/m^2.

In Figure 8c, it is evident that S2BP consistently overestimated in-situ LC_{ab}. This overestimation was characterized by a slope > 1 and a positive bias (slope = 1.04, bias = 2.09 $\mu g/cm^2$). However, the S2BP estimates for LC_{ab} were relatively accurate, with an RMSE of 60.85 $\mu g/cm^2$ and an R^2 of 0.62.

In terms of CWC accuracy, Figure 8d indicates that S2BP systematically underestimated in-situ measurements of CWC. The underestimation corresponded to both a slope < 1 and a negative bias (slope = 0.66, bias = −0.002 g/cm^2). While the S2BP-derived CWC estimates exhibited an acceptable level of uncertainty (RMSE = 0.02 g/cm^2, NSE = 0.46, R^2 = 0.51), they displayed the lowest consistency with in-situ measurements among the examined biophysical variables.

Therefore, considering EQI and uncertainty metrics, S2BP had the best performance in FVC estimation and the worst performance in CWC estimation. The estimation accuracy of the four parameters was ranked as FVC > LAI > LC_{ab} > CWC.

Figure 9 depicts the temporal variations of S2BP-derived FVC, LAI, LC_{ab}, and CWC throughout the growing season. All four parameters exhibit a consistent pattern of temporal changes. The temporal variations in FVC, LAI, and LC_{ab} follow a known and accepted pattern, increasing as the plant grows and develops, peaking in the middle of the growing period, and subsequently decreasing towards the end (Figure 9a–c). However, the CWC, which is dependent on plant water content, does not seem to align with irrigation events (Figure 9d). While an increase in vegetation cover can lead to reduced soil evaporation and increased water storage, it is important to note that the plant's transpiration also increases. Therefore, the changes in the CWC should ideally reflect both the impact of irrigation and the plant's water requirements.

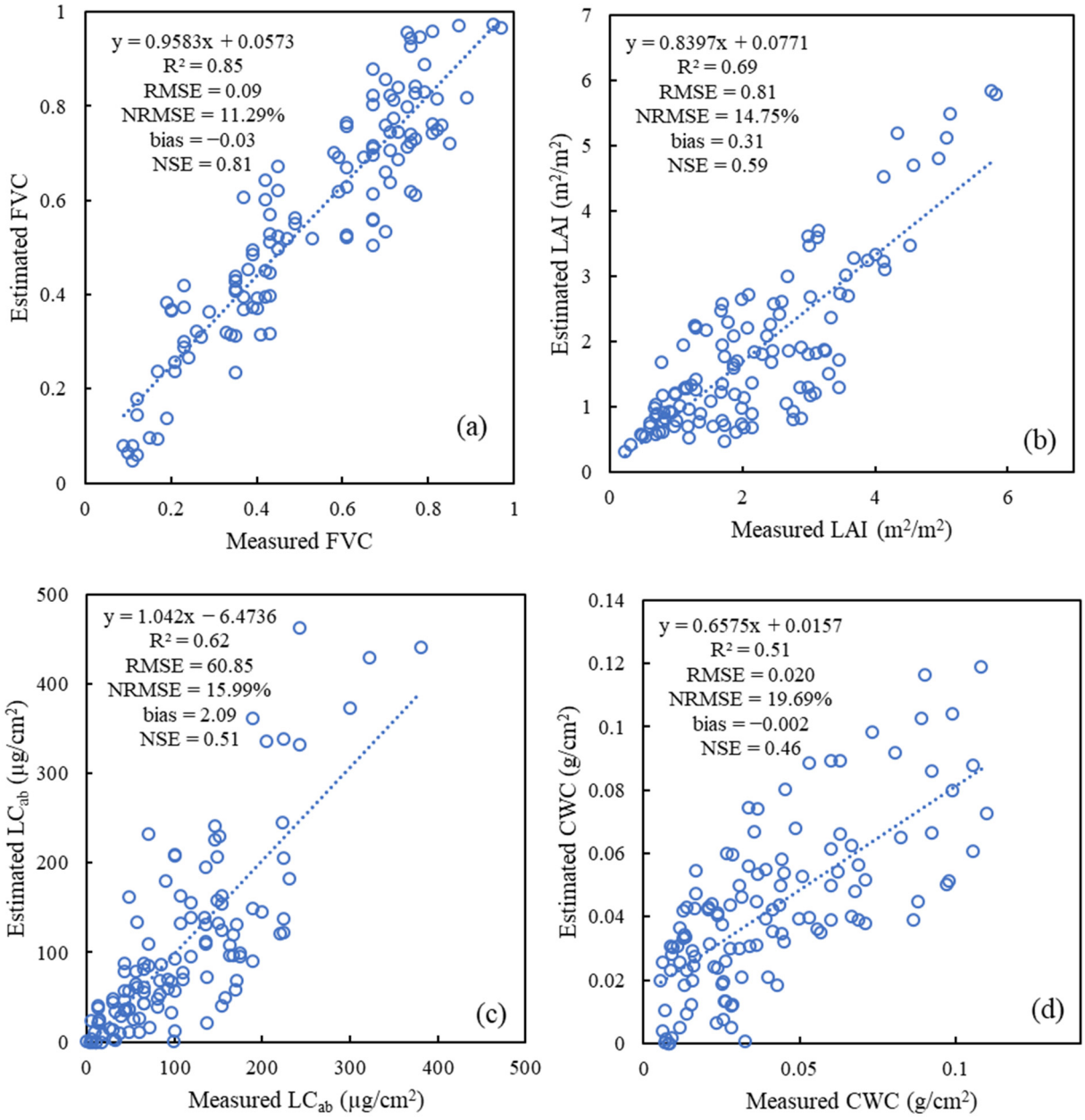

Figure 8. Scatter plot and overall linear regression function between in-situ measurements and estimates for (**a**) fractional vegetation cover (FVC), (**b**) leaf area index (LAI), (**c**) leaf chlorophyll a and b (LC_{ab}), and (**d**) canopy water content (CWC); (N = 120).

3.4. Spatial Patterns

The spatial distribution maps of the FVC, LAI, LC_{ab}, and CWC (Figure 10) with their EQI maps (Figure A1) were generated by using S2BP on 13 June, 13 July, 22 August, 1 September, 1 October, and 21 October 218. These dates include the six distinct stages of corn sowing, establishment, end of vegetative growth, flowering, senescence, and harvesting, respectively.

At the start of the growing season on 13 June, the biophysical variables exhibit low values across almost the entire field. However, as the plants become established and develop, these values increase in most parts of the field. By the end of the growing season on 21 October, the aging of the plants and their harvest had led to the lowest values of these parameters throughout the entire field. The FVC, LAI, LC_{ab}, and CWC were higher in the center of the field than in the surroundings.

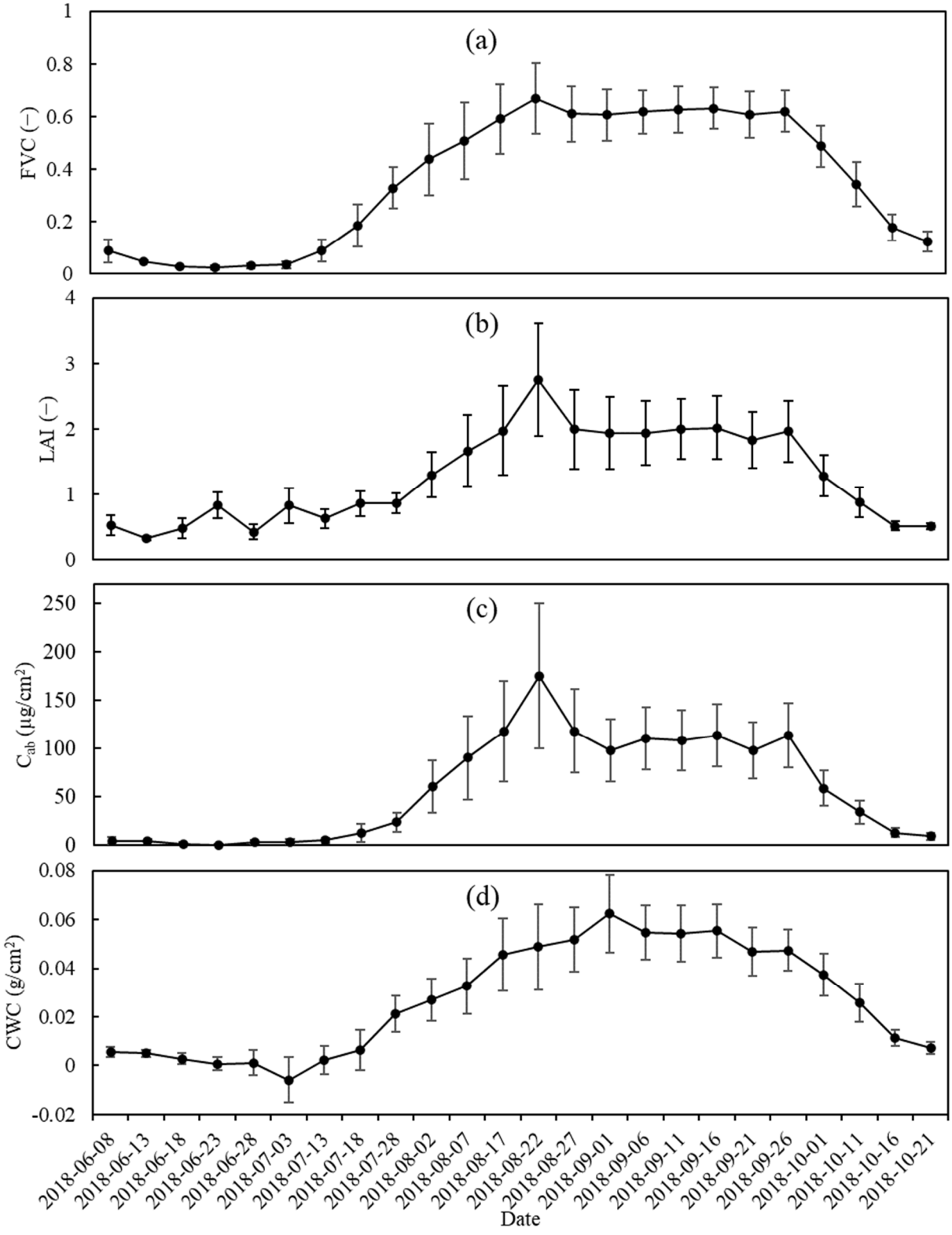

Figure 9. The temporal variation of S2BP-derived (**a**) fractional vegetation cover (FVC), (**b**) leaf area index (LAI), (**c**) leaf chlorophyll (**a**,**b**) (LC_{ab}) concentration, and (**d**) canopy water content (CWC) in the corn field during the growing season; the values presented in each date are the average of 30 ESUs.

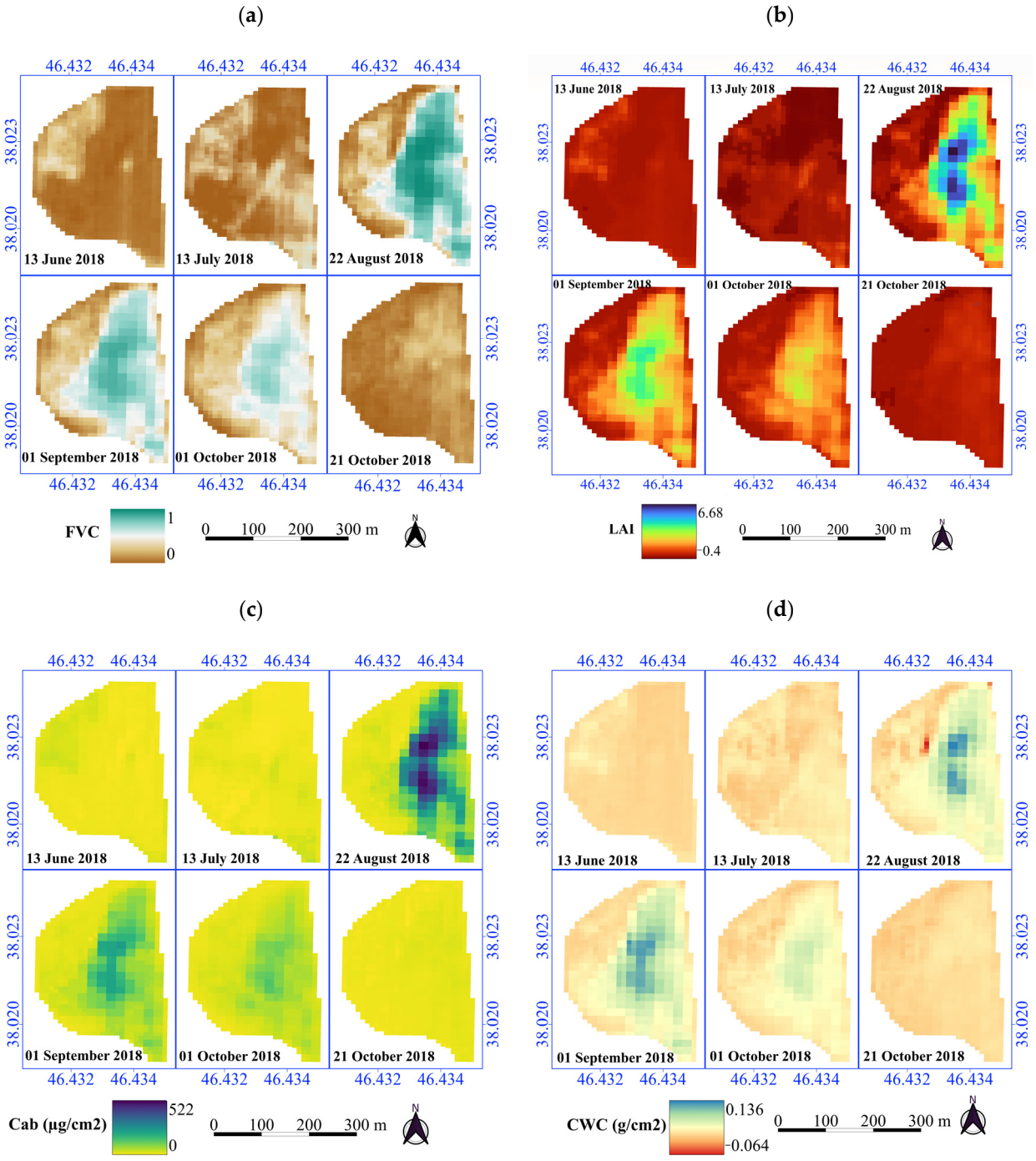

Figure 10. The spatial variations of (**a**) fractional vegetation cover (FVC), (**b**) leaf area index (LAI), (**c**) leaf chlorophyll (**a**,**b**) (LC_{ab}), and (**d**) canopy water content (CWC) at different dates of the corn growing season.

3.5. Cropland Dynamic

To examine the real-time cropland dynamics during the growing season in the field, we selected the most promising biophysical parameter investigated in this study, i.e., FVC, along with the widely recognized vegetation index, i.e., NDVI [62,63], and depicted their temporal changes (Figure 11). In addition to ground measurements, photos of vegetation cover status in the field were taken at each stage of plant growth to validate the temporal changes of these two parameters. (Figure 11). Evidently, with the onset of spring (25 March) and the warming weather, weed growth in the field commenced, leading to an increase

in NDVI and FVC. On 19 May, the field was plowed for corn cultivation, resulting in a sudden drop in the values of these two parameters. On 13 June, the plants were cultivated, and approximately 20 days later, plant germination and emergence occurred. By 13 July, vegetation cover was nearly complete in the field. The plant's vegetative growth reached its peak on 22 August, with FVC and NDVI values reaching their maximum. On 27 August, the reproductive growth began, leading to a decrease in FVC and NDVI due to the flowering. By 26 September, the reproductive growth finished, and the plant began to senesce. Plant harvesting commenced on 11 October, resulting in an immediate decrease in FVC and NDVI values. The temporal changes in LAI and LC_{ab} (Figure 9b,c) also align with these parameters, indicating the potential utility of S2BP-derived biophysical variables for monitoring real-time crop dynamics and phenology.

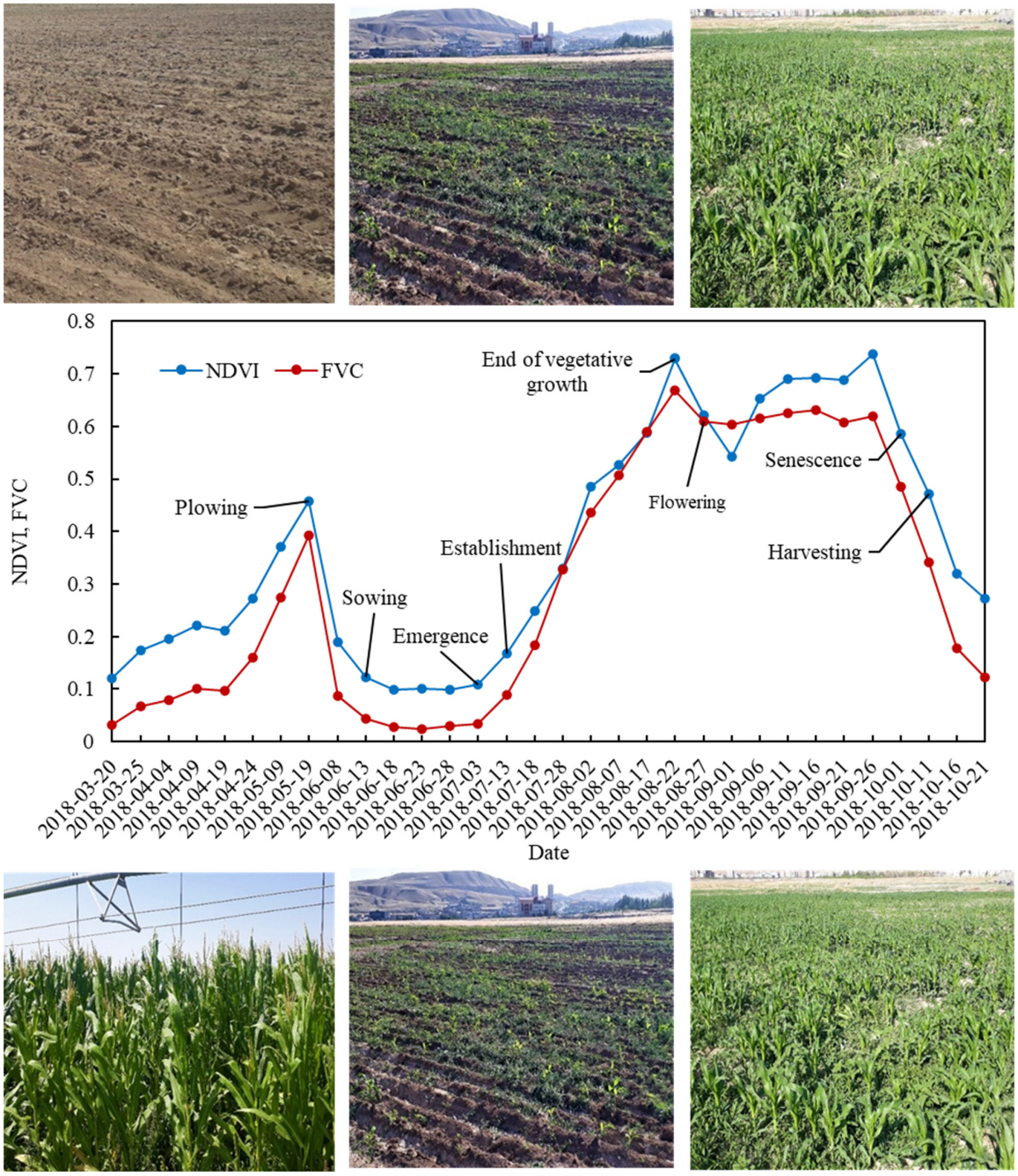

Figure 11. The temporal variation of normalized difference vegetation index (NDVI), fractional vegetation cover (FVC), and crop dynamics.

4. Discussion

This study evaluated the operational feasibility of utilizing S2BP to retrieve biophysical variables and monitor cropland dynamics throughout the entire growing season. Rigorous measures were taken to minimize potential sources of error. All measurements were precisely timed to coincide with satellite imaging, and efforts were made to utilize cloud-free and shadow-free Sentinel-2 images as inputs for S2BP. The in-situ measurements covered the period from crop establishment to approximately senescence, suggesting they are useful for assessing the S2BP for both low and high vegetation covers. Additionally, atmospheric correction was conducted using the exclusive Sen2Cor algorithm for Sentinel 2 images. Despite these efforts, the estimation quality indicators revealed uncertainties in estimating LAI, LC_{ab}, and CWC, despite S2BP's strong performance in estimating FVC. For LAI, LC_{ab}, and CWC, over 60% of the examined pixels during the plant growth period had inputs that were out-of-range. The out-of-range inputs were influenced by various factors such as cloud contamination, shadow, and poor atmospheric correction, as noted by [45]. In related studies, poor atmospheric correction [64,65] and uncertainties caused by the trained neural network [48] have been reported as the reasons for the inputs being out of range. Furthermore, in over 35% of the pixels, the output values for LC_{ab} and CWC were out-of-range. Of particular concern is the method's flagging of zero values for LC_{ab} and CWC in soil pixels as out-of-range, despite these values being normal for soil. This limitation is a drawback, as it fails to recognize that observing zero values for these parameters in the soil is not abnormal. However, it is worth noting that in some soil pixels, negative CWC values were correctly flagged as out-of-range. An additional challenge is that S2BP cannot separate the contribution of soil and vegetation from the spectral reflectance in the mixed pixels.

The accuracy metrics derived from comparing estimates and in-situ measurements also revealed uncertainties for biophysical variables, although not to the same extent as the estimation quality indicators. According to the algorithm evaluation conducted by [45], the theoretical performance described by RMSE was 0.04 for FVC, 0.81 m^2/m^2 for LAI, 56.29 $\mu g/cm^2$ for LC_{ab}, and 0.03 g/cm^2 for CWC. This explains why FVC and LAI estimates showed better agreement with in-situ measurements than LC_{ab} and CWC estimates. In previous studies on the S2BP performance, the uncertainty of FVC was reported to be 0.10–0.19 for corn [47,48] and 0.01–0.24 for other crops [47,48,64]. For LAI estimates, the uncertainty was generally 0.83–1.24 m^2/m^2 for corn [47,48] and 0.38–1.84 m^2/m^2 for other crops [6,47,48,66,67]. The uncertainty of LC_{ab} estimates was 12.69 $\mu g/cm^2$ for other crops [6]. As for CWC estimates, the uncertainty was generally 0.014 g/cm^2 for corn [47] and 0.007–0.083 g/cm^2 for other crops [47,64,68]. In comparison to similar studies, this research utilized ground validation data with greater temporal coverage during the growing season to evaluate S2BP estimates. Overall, our validation results are consistent with the findings of other studies and offer more accurate estimates for FVC and LAI and less accurate estimates for CWC compared to the studies conducted on corn. No study has been carried out regarding the estimation of corn LC_{ab} using S2BP.

The spatial patterns of biophysical variables revealed that the FVC, LAI, LC_{ab}, and CWC were higher in the center of the field than in the surroundings. In fields irrigated by a center pivot system, the central areas often receive more water due to higher water pressure and flow in the nozzles closer to the center compared to the outermost nozzles. Despite the system settings being designed to ensure uniform irrigation, there is a noticeable lack of uniformity in the studied field. This is further compounded by surface irrigation in addition to center-pivot irrigation, resulting in the southeast part of the field consistently exhibiting higher FVC, LAI, LC_{ab}, and CWC. Other contributing factors to these spatial variations may include uneven fertilizer distribution, inconsistent tillage practices, or variability in surface soil type.

Examining the spatial and temporal variations of FVC, LAI, and LC_{ab} reveals their alignment with field activities and events (Figures 9 and 11). These parameters are closely linked to the greenness, density, and overall health of vegetation cover. Any field activity

or event that alters these parameters or introduces biotic or abiotic stresses will consequently impact these parameters [69]. Consequently, monitoring the temporal and spatial changes in these parameters can serve as a valuable tool for assessing plant dynamics and health. This information can be instrumental in precision farming, assisting in the optimization of variable agricultural inputs such as fertilizers, pesticides, and water, ultimately enhancing productivity.

A limitation of this research is the lack of a comprehensive in situ database of biophysical variables to validate S2BP at the national, regional, and global scales. Having various field data with consistent measurement criteria allows for a better understanding of the performance of long-term S2BP estimates for different biophysical variables (FVC, LAI, LC_{ab}, and CWC) and vegetation types (crops, forests, and grasses). The best approach is to incorporate more ground measurements from well-distributed field campaigns for various vegetation types. To ensure reliable evaluation results, it would be useful to generate new on-site reference datasets and establish globally distributed research networks. Site-based measurement networks offer benefits for validating decametric products due to the proximity of ground measurements to the pixel grid of products. Thus, a greater number of ground measurements encompassing the products can be gathered from the worldwide network of sites. These measurements can then enhance the quantification of uncertainties, especially regarding the performance of time series associated with Sentinel-2 biophysical estimates. In contrast to commonly used coarse-resolution products, user communities can generate biophysical estimates using S2BP. Integrating Sentinel-2 MSI with other satellite sensors of varying spatial resolutions, such as Landsat-8 and Landsat-9 OLI (Harmonized Landsat Sentinel-2) [70], shows potential for producing temporally continuous biophysical variables at a high spatial resolution.

Another limitation is the weakness of the algorithm and training database generated in S2BP. For instance, the input being out-of-range (EQI = 1) in a considerable portion of the pixels (over 60% for LAI, LC_{ab}, and CWC variables) serves as evidence thereof. Hence, enhancing the algorithm for S2BP estimates is warranted.

The occurrence of mixed pixels throughout the plant growth season poses another challenge to the accurate estimation of biophysical parameters with S2BP. The S2BP algorithm struggles to distinguish the contributions of end members (soil and vegetation) in a mixed pixel. Techniques such as spectral unmixing can assist in addressing this issue.

5. Conclusions

This study delved into the potential of the Sentinel-2 biophysical processor (S2BP) to accurately estimate biophysical variables (FVC, LAI, LCab, and CWC) and intricately monitor cropland dynamics across a designated agricultural site in Tabriz, Iran. Quantitative and qualitative validations of FVC, LAI, LC_{ab}, and CWC estimates were employed during the corn growing season using all ground observations and estimation quality indicators (EQIs), respectively. The results show that, according to EQI, the best retrievals were obtained for FVC in around 99.9% of the analyzed pixels during the growth season. However, for LAI, LC_{ab}, and CWC, a significant percentage (exceeding 60%) of the examined pixels had out-of-range inputs. Additionally, over 35% of the pixels showed out-of-range outputs for LC_{ab} and CWC. Given uncertainty metrics, the estimates for FVC, LAI, and LC_{ab} agreed well with ground measurements (RMSE of 0.09, 0.81 m^2/m^2, and 60.85 $\mu g/cm^2$, and R^2 of 0.85, 0.69, and 0.62, respectively), but there was a discrepancy for CWC estimates (RMSE = 0.02 g/cm^2 and R^2 = 0.51). The temporal variations of FVC, LAI, and LC_{ab} were consistent with field-scale events and crop dynamics. Overall, the present study demonstrates the feasibility of employing Sentinel-2 satellite data and S2BP to meticulously monitor biophysical variables and discern cropland dynamics for precision agriculture.

This study suggests that the robustness of the findings could be amplified by incorporating a pixel identification algorithm, such as spectral unmixing, into the S2BP algorithm. Additional quantitative assessment of agricultural production events and re-

trievable variables across diverse landscape and climate contexts is essential in investigating the wide-scale applicability of this approach.

In addition to using biophysical variables for real-time monitoring of crop dynamics and farm management in precision agriculture, operational initiatives based on S2BP, like Web-GIS technologies for web mapping applications and geolocation solutions, can enhance resource management, including water. Remote sensing-based decision support systems are another operational application that can utilize S2BP to support satellite-based agricultural services. Forecasting photosynthesis and crop yield through biophysical variables is another valuable application that can be considered. S2BP can offer biophysical variables as quality inputs for crop growth models like agricultural production systems simulator (APSIM) and AquaCrop. Exploring the linkage and implementation of these tools in future studies could be beneficial.

Author Contributions: Conceptualization, R.H. and A.M.-H.; methodology, R.H. and A.F.F.; formal analysis, R.H.; data curation, J.V.; writing—original draft preparation, R.H.; writing—review and editing, A.M.-H. and J.V.; visualization, R.H.; supervision, A.M.-H., A.F.F. and J.V.; project administration, A.M.-H., A.F.F. and R.H. All authors have read and agreed to the published version of the manuscript.

Funding: This research received no external funding.

Data Availability Statement: No new data were created or analyzed in this study. Data sharing is not applicable to this article.

Acknowledgments: The authors thank the University of Tabriz for supporting this research and the European Union for open access funding through the ERC, FLEXINEL fund (grant no. 101086622).

Conflicts of Interest: The authors declare no conflicts of interest.

Appendix A

Figure A1 indicates the spatial variations of EQI for FVC, LAI, LC_{ab}, and CWC at six growing season stages.

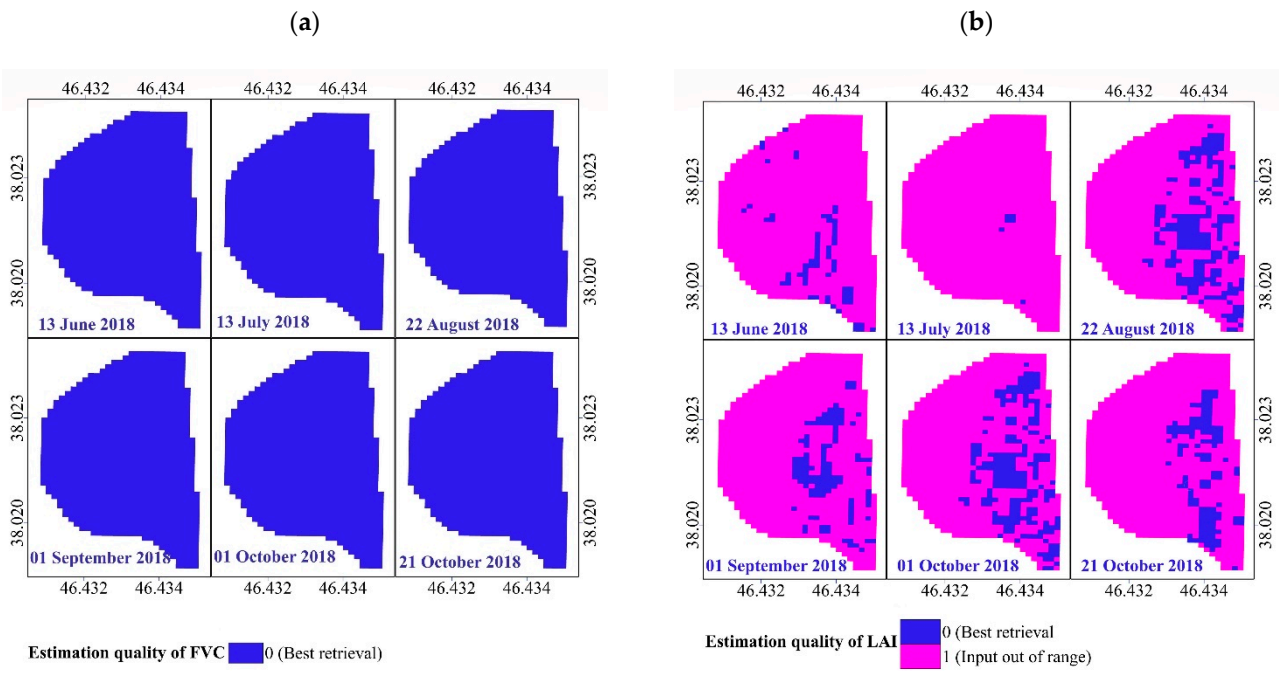

Figure A1. *Cont.*

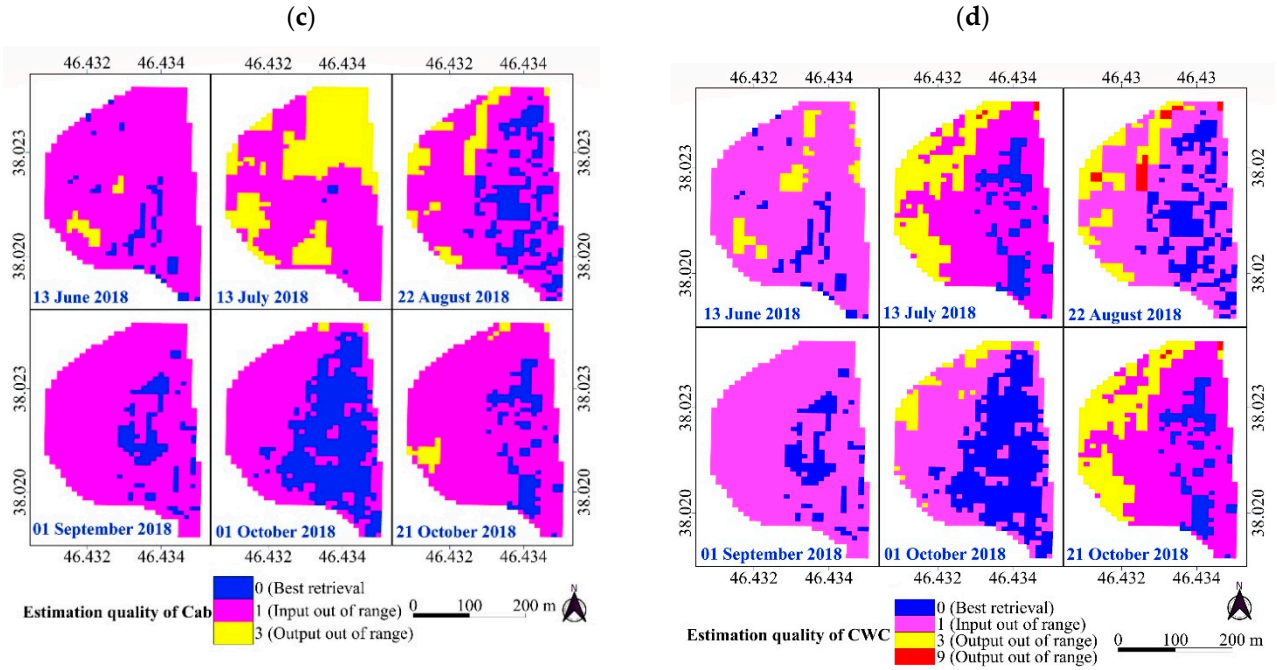

Figure A1. The spatial variations of estimation quality indicators (EQI) for (**a**) fractional vegetation cover (FVC, (**b**) leaf area index (LAI), (**c**) leaf chlorophyll a and b (LC_{ab}), and (**d**) canopy water content (CWC) at different dates of the corn growing season.

References

1. Brisco, B.; Brown, R.J.; Hirose, T.; McNairn, H.; Staenz, K. Precision Agriculture and the Role of Remote Sensing: A Review. *Can. J. Remote Sens.* **1998**, *24*, 315–327. [CrossRef]
2. Wang, K.; Franklin, S.E.; Guo, X.; Cattet, M. Remote Sensing of Ecology, Biodiversity and Conservation: A Review from the Perspective of Remote Sensing Specialists. *Sensors* **2010**, *10*, 9647–9667. [CrossRef] [PubMed]
3. Guan, K.; Wu, J.; Kimball, J.S.; Anderson, M.C.; Frolking, S.; Li, B.; Hain, C.R.; Lobell, D.B. The Shared and Unique Values of Optical, Fluorescence, Thermal and Microwave Satellite Data for Estimating Large-Scale Crop Yields. *Remote Sens. Environ.* **2017**, *199*, 333–349. [CrossRef]
4. Houborg, R.; Soegaard, H.; Boegh, E. Combining Vegetation Index and Model Inversion Methods for the Extraction of Key Vegetation Biophysical Parameters Using Terra and Aqua MODIS Reflectance Data. *Remote Sens. Environ.* **2007**, *106*, 39–58. [CrossRef]
5. Huang, J.; Ma, H.; Su, W.; Zhang, X.; Huang, Y.; Fan, J.; Wu, W. Jointly Assimilating MODIS LAI and ET Products into the SWAP Model for Winter Wheat Yield Estimation. *IEEE J. Sel. Top. Appl. Earth Obs. Remote Sens.* **2015**, *8*, 4060–4071. [CrossRef]
6. Xie, Q.; Dash, J.; Huete, A.; Jiang, A.; Yin, G.; Ding, Y.; Peng, D.; Hall, C.C.; Brown, L.; Shi, Y. Retrieval of Crop Biophysical Parameters from Sentinel-2 Remote Sensing Imagery. *Int. J. Appl. Earth Obs. Geoinf.* **2019**, *80*, 187–195. [CrossRef]
7. Deardorff, J.W. Efficient Prediction of Ground Surface Temperature and Moisture, with Inclusion of a Layer of Vegetation. *J. Geophys. Res. Ocean.* **1978**, *83*, 1889–1903. [CrossRef]
8. Jiang, M.; Tian, S.; Zheng, Z.; Zhan, Q.; He, Y. Human Activity Influences on Vegetation Cover Changes in Beijing, China, from 2000 to 2015. *Remote Sens.* **2017**, *9*, 271. [CrossRef]
9. Jia, K.; Liang, S.; Gu, X.; Baret, F.; Wei, X.; Wang, X.; Yao, Y.; Yang, L.; Li, Y. Fractional Vegetation Cover Estimation Algorithm for Chinese GF-1 Wide Field View Data. *Remote Sens. Environ.* **2016**, *177*, 184–191. [CrossRef]
10. Tong, S.; Zhang, J.; Ha, S.; Lai, Q.; Ma, Q. Dynamics of Fractional Vegetation Coverage and Its Relationship with Climate and Human Activities in Inner Mongolia, China. *Remote Sens.* **2016**, *8*, 776. [CrossRef]
11. Fang, H.; Baret, F.; Plummer, S.; Schaepman-Strub, G. An Overview of Global Leaf Area Index (LAI): Methods, Products, Validation, and Applications. *Rev. Geophys.* **2019**, *57*, 739–799. [CrossRef]
12. GCOS. *Systematic Observation Requirements for Satellite-Based Products for Climate Supplemental Details to the Satellite-Based Component of the Implementation Plan for the Global Observing System for Climate in Support of the UNFCCC-2011 Update, Supplemental*; World Meteorological Organization: Geneva, Switzerland, 2011.
13. Fang, H.; Liang, S. Leaf Area Index Models. In Encyclopedia of Ecology; Jørgensen, S.E., Fath, B.D., Eds.; Elsevier Science, 2008; pp. 2139–2148, ISBN 978-0-08-045405-4.
14. Allen, R.G.; Pereira, L.S.; Raes, D.; Smith, M. *Crop Evapotranspiration-Guidelines for Computing Crop Water Requirements-FAO Irrigation and Drainage Paper 56*; FAO: Rome, Italy, 1998; Volume 300, p. D05109.

15. Darvishzadeh, R.; Skidmore, A.; Schlerf, M.; Atzberger, C. Inversion of a Radiative Transfer Model for Estimating Vegetation LAI and Chlorophyll in a Heterogeneous Grassland. *Remote Sens. Environ.* **2008**, *112*, 2592–2604. [CrossRef]
16. Abdullah, H.; Darvishzadeh, R.; Skidmore, A.K.; Groen, T.A.; Heurich, M. European Spruce Bark Beetle (*Ips typographus* L.) Green Attack Affects Foliar Reflectance and Biochemical Properties. *Int. J. Appl. Earth Obs. Geoinf.* **2018**, *64*, 199–209. [CrossRef]
17. Inoue, Y.; Sakaiya, E.; Zhu, Y.; Takahashi, W. Diagnostic Mapping of Canopy Nitrogen Content in Rice Based on Hyperspectral Measurements. *Remote Sens. Environ.* **2012**, *126*, 210–221. [CrossRef]
18. Féret, J.B.; Gitelson, A.A.; Noble, S.D.; Jacquemoud, S. PROSPECT-D: Towards Modeling Leaf Optical Properties through a Complete Lifecycle. *Remote Sens. Environ.* **2017**, *193*, 204–215. [CrossRef]
19. Carter, G.A. Responses of Leaf Spectral Reflectance to Plant Stress. *Am. J. Bot.* **1993**, *80*, 239–243. [CrossRef]
20. Stimson, H.C.; Breshears, D.D.; Ustin, S.L.; Kefauver, S.C. Spectral Sensing of Foliar Water Conditions in Two Co-Occurring Conifer Species: Pinus Edulis and Juniperus Monosperma. *Remote Sens. Environ.* **2005**, *96*, 108–118. [CrossRef]
21. Peñuelas, J.; Filella, I.; Biel, C.; Serrano, L.; Save, R. The Reflectance at the 950–970 Nm Region as an Indicator of Plant Water Status. *Int. J. Remote Sens.* **1993**, *14*, 1887–1905. [CrossRef]
22. Marusig, D.; Petruzzellis, F.; Tomasella, M.; Napolitano, R.; Altobelli, A.; Nardini, A. Correlation of Field-Measured and Remotely Sensed Plant Water Status as a Tool to Monitor the Risk of Drought-Induced Forest Decline. *Forests* **2020**, *11*, 77. [CrossRef]
23. Yi, Q.; Wang, F.; Bao, A.; Jiapaer, G. Leaf and Canopy Water Content Estimation in Cotton Using Hyperspectral Indices and Radiative Transfer Models. *Int. J. Appl. Earth Obs. Geoinf.* **2014**, *33*, 67–75. [CrossRef]
24. Farhadi, H.; Najafzadeh, M. Flood Risk Mapping by Remote Sensing Data and Random Forest Technique. *Water* **2021**, *13*, 3115. [CrossRef]
25. Hantson, S.; Arneth, A.; Harrison, S.P.; Kelley, D.I.; Prentice, I.C.; Rabin, S.S.; Archibald, S.; Mouillot, F.; Arnold, S.R.; Artaxo, P. The Status and Challenge of Global Fire Modelling. *Biogeosciences* **2016**, *13*, 3359–3375. [CrossRef]
26. Ruffault, J.; Limousin, J.; Pimont, F.; Dupuy, J.; De Càceres, M.; Cochard, H.; Mouillot, F.; Blackman, C.J.; Torres-Ruiz, J.M.; Parsons, R.A. Plant Hydraulic Modelling of Leaf and Canopy Fuel Moisture Content Reveals Increasing Vulnerability of a Mediterranean Forest to Wildfires under Extreme Drought. *New Phytol.* **2023**, *237*, 1256–1269. [CrossRef] [PubMed]
27. Abdelbaki, A.; Udelhoven, T. A Review of Hybrid Approaches for Quantitative Assessment of Crop Traits Using Optical Remote Sensing: Research Trends and Future Directions. *Remote Sens.* **2022**, *14*, 3515. [CrossRef]
28. Mohammad Ali, A.; Darvishzadeh, R.; Skidmore, A.; Gara, T.W.; O'Connor, B.; Roeoesli, C.; Heurich, M.; Paganini, M. Comparing Methods for Mapping Canopy Chlorophyll Content in a Mixed Mountain Forest Using Sentinel-2 Data. *Int. J. Appl. Earth Obs. Geoinf.* **2020**, *87*, 102037. [CrossRef]
29. Verrelst, J.; Camps-Valls, G.; Muñoz-Marí, J.; Rivera, J.P.; Veroustraete, F.; Clevers, J.G.P.W.; Moreno, J. Optical Remote Sensing and the Retrieval of Terrestrial Vegetation Bio-Geophysical Properties–A Review. *ISPRS J. Photogramm. Remote Sens.* **2015**, *108*, 273–290. [CrossRef]
30. Lázaro-Gredilla, M.; Titsias, M.K.; Verrelst, J.; Camps-Valls, G. Retrieval of Biophysical Parameters with Heteroscedastic Gaussian Processes. *IEEE Geosci. Remote Sens. Lett.* **2013**, *11*, 838–842. [CrossRef]
31. Cui, S.; Zhou, K. A Comparison of the Predictive Potential of Various Vegetation Indices for Leaf Chlorophyll Content. *Earth Sci. Inform.* **2017**, *10*, 169–181. [CrossRef]
32. Liang, L.; Qin, Z.; Zhao, S.; Di, L.; Zhang, C.; Deng, M.; Lin, H.; Zhang, L.; Wang, L.; Liu, Z. Estimating Crop Chlorophyll Content with Hyperspectral Vegetation Indices and the Hybrid Inversion Method. *Int. J. Remote Sens.* **2016**, *37*, 2923–2949. [CrossRef]
33. Rocha, A.D.; Groen, T.A.; Skidmore, A.K.; Darvishzadeh, R.; Willemen, L. The Naïve Overfitting Index Selection (NOIS): A New Method to Optimize Model Complexity for Hyperspectral Data. *ISPRS J. Photogramm. Remote Sens.* **2017**, *133*, 61–74. [CrossRef]
34. Verrelst, J.; Malenovský, Z.; Van der Tol, C.; Camps-Valls, G.; Gastellu-Etchegorry, J.-P.; Lewis, P.; North, P.; Moreno, J. Quantifying Vegetation Biophysical Variables from Imaging Spectroscopy Data: A Review on Retrieval Methods. *Surv. Geophys.* **2019**, *40*, 589–629. [CrossRef] [PubMed]
35. Rosso, P.; Nendel, C.; Gilardi, N.; Udroiu, C.; Chlebowski, F. Processing of Remote Sensing Information to Retrieve Leaf Area Index in Barley: A Comparison of Methods. *Precis. Agric.* **2022**, *23*, 1449–1472. [CrossRef]
36. Bacour, C.; Baret, F.; Béal, D.; Weiss, M.; Pavageau, K. Neural Network Estimation of LAI, FAPAR, FCover and LAI× Cab, from Top of Canopy MERIS Reflectance Data: Principles and Validation. *Remote Sens. Environ.* **2006**, *105*, 313–325. [CrossRef]
37. Zheng, G.; Moskal, L.M. Retrieving Leaf Area Index (LAI) Using Remote Sensing: Theories, Methods and Sensors. *Sensors* **2009**, *9*, 2719–2745. [CrossRef]
38. Combal, B.; Baret, F.; Weiss, M.; Trubuil, A.; Macé, D.; Pragnère, A.; Myneni, R.; Knyazikhin, Y.; Wang, L. Retrieval of Canopy Biophysical Variables from Bidirectional Reflectance: Using Prior Information to Solve the Ill-Posed Inverse Problem. *Remote Sens. Environ.* **2003**, *84*, 1–15. [CrossRef]
39. Scales, J.A.; Tenorio, L. Prior Information and Uncertainty in Inverse Problems. *Geophysics* **2001**, *66*, 389–397. [CrossRef]
40. Casa, R.; Baret, F.; Buis, S.; Lopez-Lozano, R.; Pascucci, S.; Palombo, A.; Jones, H.G. Estimation of Maize Canopy Properties from Remote Sensing by Inversion of 1-D and 4-D Models. *Precis. Agric.* **2010**, *11*, 319–334. [CrossRef]
41. Verrelst, J.; Rivera, J.P.; Veroustraete, F.; Muñoz-Marí, J.; Clevers, J.G.P.W.; Camps-Valls, G.; Moreno, J. Experimental Sentinel-2 LAI Estimation Using Parametric, Non-Parametric and Physical Retrieval Methods–A Comparison. *ISPRS J. Photogramm. Remote Sens.* **2015**, *108*, 260–272. [CrossRef]

42. Adeluyi, O.; Harris, A.; Verrelst, J.; Foster, T.; Clay, G.D. Estimating the Phenological Dynamics of Irrigated Rice Leaf Area Index Using the Combination of PROSAIL and Gaussian Process Regression. *Int. J. Appl. Earth Obs. Geoinf.* **2021**, *102*, 102454. [CrossRef] [PubMed]
43. Sinha, S.K.; Padalia, H.; Dasgupta, A.; Verrelst, J.; Rivera, J.P. Estimation of Leaf Area Index Using PROSAIL Based LUT Inversion, MLRA-GPR and Empirical Models: Case Study of Tropical Deciduous Forest Plantation, North India. *Int. J. Appl. Earth Obs. Geoinf.* **2020**, *86*, 102027. [CrossRef] [PubMed]
44. Jacquemoud, S.; Verhoef, W.; Baret, F.; Bacour, C.; Zarco-Tejada, P.J.; Asner, G.P.; François, C.; Ustin, S.L. PROSPECT + SAIL Models: A Review of Use for Vegetation Characterization. *Remote Sens. Environ.* **2009**, *113*, S56–S66. [CrossRef]
45. Weiss, M.; Baret, F. *S2ToolBox Level 2 Products: LAI, FAPAR, FCOVER*; Institut National de la Recherche Agronomique (INRA): Avignon, France, 2016.
46. Defourny, P.; Bontemps, S.; Bellemans, N.; Cara, C.; Dedieu, G.; Guzzonato, E.; Hagolle, O.; Inglada, J.; Nicola, L.; Rabaute, T.; et al. Near Real-Time Agriculture Monitoring at National Scale at Parcel Resolution: Performance Assessment of the Sen2-Agri Automated System in Various Cropping Systems around the World. *Remote Sens. Environ.* **2019**, *221*, 551–568. [CrossRef]
47. Djamai, N.; Fernandes, R.; Weiss, M.; McNairn, H.; Goïta, K. Validation of the Sentinel Simplified Level 2 Product Prototype Processor (SL2P) for Mapping Cropland Biophysical Variables Using Sentinel-2/MSI and Landsat-8/OLI Data. *Remote Sens. Environ.* **2019**, *225*, 416–430. [CrossRef]
48. Hu, Q.; Yang, J.; Xu, B.; Huang, J.; Memon, M.S.; Yin, G.; Zeng, Y.; Zhao, J.; Liu, K. Evaluation of Global Decametric-Resolution LAI, FAPAR and FVC Estimates Derived from Sentinel-2 Imagery. *Remote Sens.* **2020**, *12*, 912. [CrossRef]
49. Zhang, M.; Su, W.; Fu, Y.; Zhu, D.; Xue, J.-H.; Huang, J.; Wang, W.; Wu, J.; Yao, C. Super-Resolution Enhancement of Sentinel-2 Image for Retrieving LAI and Chlorophyll Content of Summer Corn. *Eur. J. Agron.* **2019**, *111*, 125938. [CrossRef]
50. Baret, F.; Weiss, M.; Allard, D.; Garrigues, S.; Leroy, M.; Jeanjean, H.; Fernandes, R.; Myneni, R.; Privette, J.; Morisette, J.; et al. VALERI: A Network of Sites and a Methodology for the Validation of Medium Spatial Resolution Land Satellite Products. Available online: http://w3.avignon.inra.fr/valeri/ (accessed on 18 November 2023).
51. McNairn, H.; Jackson, T.J.; Powers, J.; Bélair, S.; Berg, A.; Bullock, P.; Colliander, A.; Cosh, M.H.; Kim, S.-B.; Magagi, R. SMAPVEX16 Database Report. 2016. Available online: http://smapvex16-mb.espaceweb.usherbrooke.ca/documents/SMAPVEX16_database_report2020170131.pdf (accessed on 25 December 2023).
52. European Space Agency SPARC Data Acquisition Report. Available online: https://earth.esa.int/eogateway/documents/20142/37627/SPARC-2004-data-acquisition-report.pdf (accessed on 25 December 2023).
53. Amri, M.; Abbes, Z.; Trabelsi, I.; Ghanem, M.E.; Mentag, R.; Kharrat, M. Chlorophyll Content and Fluorescence as Physiological Parameters for Monitoring Orobanche Foetida Poir. Infection in Faba Bean. *PLoS ONE* **2021**, *16*, e0241527. [CrossRef] [PubMed]
54. Yebra, M.; Dennison, P.E.; Chuvieco, E.; Riaño, D.; Zylstra, P.; Hunt, E.R., Jr.; Danson, F.M.; Qi, Y.; Jurdao, S. A Global Review of Remote Sensing of Live Fuel Moisture Content for Fire Danger Assessment: Moving towards Operational Products. *Remote Sens. Environ.* **2013**, *136*, 455–468. [CrossRef]
55. European Space Agency. *Sentinel-2 User Handbook. ESA Standard Document*; European Space Agency: Paris, France, 2015.
56. Bioucas-Dias, J.M.; Plaza, A.; Dobigeon, N.; Parente, M.; Du, Q.; Gader, P.; Chanussot, J. Hyperspectral Unmixing Overview: Geometrical, Statistical, and Sparse Regression-Based Approaches. *IEEE J. Sel. Top. Appl. Earth Obs. Remote Sens.* **2012**, *5*, 354–379. [CrossRef]
57. Richter, R.; Louis, J.; Müller-Wilm, U. *Sentinel-2 MSI—Level 2A Products Algorithm Theoretical Basis Document*; Special Publication; European Space Agency: Paris, France, 2012.
58. Hyndman, R.J.; Koehler, A.B. Another Look at Measures of Forecast Accuracy. *Int. J. Forecast.* **2006**, *22*, 679–688. [CrossRef]
59. Von Luxburg, U.; Schölkopf, B. Statistical Learning Theory: Models, Concepts, and Results. In *Handbook of the History of Logic*; Elsevier: Amsterdam, The Netherlands, 2011; Volume 10, pp. 651–706. ISBN 1874-5857.
60. Nash, J.E.; Sutcliffe, J. V River Flow Forecasting through Conceptual Models Part I—A Discussion of Principles. *J. Hydrol.* **1970**, *10*, 282–290. [CrossRef]
61. Draper, N.R.; Smith, H. *Applied Regression Analysis*; John Wiley & Sons: Hoboken, NJ, USA, 1998; Volume 326, ISBN 0471170828.
62. Li, C.; Li, H.; Li, J.; Lei, Y.; Li, C.; Manevski, K.; Shen, Y. Using NDVI Percentiles to Monitor Real-Time Crop Growth. *Comput. Electron. Agric.* **2019**, *162*, 357–363. [CrossRef]
63. Shammi, S.A.; Meng, Q. Use Time Series NDVI and EVI to Develop Dynamic Crop Growth Metrics for Yield Modeling. *Ecol. Indic.* **2021**, *121*, 107124. [CrossRef]
64. Djamai, N.; Zhong, D.; Fernandes, R.; Zhou, F. Evaluation of Vegetation Biophysical Variables Time Series Derived from Synthetic Sentinel-2 Images. *Remote Sens.* **2019**, *11*, 1547. [CrossRef]
65. Li, Y.; Chen, J.; Ma, Q.; Zhang, H.K.; Liu, J. Evaluation of Sentinel-2A Surface Reflectance Derived Using Sen2Cor in North America. *IEEE J. Sel. Top. Appl. Earth Obs. Remote Sens.* **2018**, *11*, 1997–2021. [CrossRef]
66. Pasqualotto, N.; D'Urso, G.; Bolognesi, S.F.; Belfiore, O.R.; Van Wittenberghe, S.; Delegido, J.; Pezzola, A.; Winschel, C.; Moreno, J. Retrieval of Evapotranspiration from Sentinel-2: Comparison of Vegetation Indices, Semi-Empirical Models and SNAP Biophysical Processor Approach. *Agronomy* **2019**, *9*, 663. [CrossRef]
67. Upreti, D.; Huang, W.; Kong, W.; Pascucci, S.; Pignatti, S.; Zhou, X.; Ye, H.; Casa, R. A Comparison of Hybrid Machine Learning Algorithms for the Retrieval of Wheat Biophysical Variables from Sentinel-2. *Remote Sens.* **2019**, *11*, 481. [CrossRef]

68. Pan, H.; Chen, Z.; Ren, J.; Li, H.; Wu, S. Modeling Winter Wheat Leaf Area Index and Canopy Water Content with Three Different Approaches Using Sentinel-2 Multispectral Instrument Data. *IEEE J. Sel. Top. Appl. Earth Obs. Remote Sens.* **2018**, *12*, 482–492. [CrossRef]
69. Li, Y.; Sun, J.; Wang, M.; Guo, J.; Wei, X.; Shukla, M.K.; Qi, Y. Spatiotemporal Variation of Fractional Vegetation Cover and Its Response to Climate Change and Topography Characteristics in Shaanxi Province, China. *Appl. Sci.* **2023**, *13*, 11532. [CrossRef]
70. Claverie, M.; Ju, J.; Masek, J.G.; Dungan, J.L.; Vermote, E.F.; Roger, J.-C.; Skakun, S.V.; Justice, C. The Harmonized Landsat and Sentinel-2 Surface Reflectance Data Set. *Remote Sens. Environ.* **2018**, *219*, 145–161. [CrossRef]